CANCER

# Leveraging gene therapy to achieve long-term continuous or controllable expression of biotherapeutics

**Timothy P. Cripe[1,2]*†, Brian Hutzen[1]†, Mark A. Currier[1]†, Chun-Yu Chen[1]†, Andrea M. Glaspell[1], Grace C. Sullivan[1], Julia M. Hurley[1], Mackenzie R. Deighen[1], Akila S. Venkataramany[1,3], Xiaokui Mo[4], Joseph R. Stanek[2], Anthony R. Miller[5], Saranga Wijeratne[5], Vincent Magrini[5], Elaine R. Mardis[5], Jerry R. Mendell[6], Dawn S. Chandler[1,3], Pin-Yi Wang[1]**

Copyright © 2022 The Authors, some rights reserved; exclusive licensee American Association for the Advancement of Science. No claim to original U.S. Government Works. Distributed under a Creative Commons Attribution NonCommercial License 4.0 (CC BY-NC).

**T cells redirected to cancer cells either via a chimeric antigen receptor (CAR-T) or a bispecific molecule have been breakthrough technologies; however, CAR-T cells require individualized manufacturing and bispecifics generally require continuous infusions. We created an off-the-shelf, single-dose solution for achieving prolonged systemic serum levels of protein immunotherapeutics via adeno-associated virus (AAV) gene transfer. We demonstrate proof of principle in a CD19$^+$ lymphoma xenograft model using a single intravenous dose of AAV expressing a secreted version of blinatumomab, which could serve as a universal alternative for CD19 CAR-T cell therapy. In addition, we created an inducible version using an exon skipping strategy and achieved repeated, on-demand expression up to at least 36 weeks after AAV injection. Our system could be considered for short-term and/or repeated expression of other transgenes of interest for noncancer applications.**

## INTRODUCTION

Most medications are administered on an intermittent schedule, resulting in pharmacokinetic peaks and troughs. Great efforts are expended to find dosages and schedules that minimize time spent outside of the therapeutic window, resulting in more frequent doses for drugs with shorter half-lives, inevitably with troughs below efficacious levels. These troughs are a particular challenge for cancer, as they enable periods of cancer regrowth and development of drug resistance. Furthermore, drugs with extremely short half-lives require continuous infusions, which are cumbersome as they require frequent hospital or home care visits for bag or syringe changes, pose vascular access challenges, and create risk for infections. Diseases such as cancer, cardiovascular disease, and chronic pain require long-term therapy, and others such as rheumatologic diseases require intermittent therapy over long periods of time.

Recent advances in gene therapy for correction of monogenic disorders have led to successful replacement of missing or defective genes, yielding constant expression of a transgene for months to years. We sought to determine whether gene therapy could also potentially solve the problems of peaks and troughs for protein-based medicines by enabling sustained and consistent levels of therapeutics in the blood and tissue after a single dose.

[1]Center for Childhood Cancer and Blood Diseases, Abigail Wexner Research Institute at Nationwide Children's Hospital, 700 Children's Drive, Columbus, OH 43205, USA. [2]Division of Hematology/Oncology/Blood and Marrow Transplantation, Nationwide Children's Hospital, Department of Pediatrics, The Ohio State University, 700 Children's Drive, Columbus, OH 43205, USA. [3]Center for RNA Biology, The Ohio State University, 105 Biological Sciences Building, 484 West 12th Avenue, Columbus, OH 43210-1292, USA. [4]Department of Biomedical Informatics, The Ohio State University, 1585 Neil Ave, Columbus, OH 43210, USA. [5]The Steve and Cindy Rasmussen Institute for Genomic Medicine, Abigail Wexner Research Institute at Nationwide Children's Hospital, 700 Children's Drive, Columbus, OH 43205, USA. [6]Center for Gene Therapy, Abigail Wexner Research Institute at Nationwide Children's Hospital, 700 Children's Drive, Columbus, OH 43205, USA.
*Corresponding author. Email: timothy.cripe@nationwidechildrens.org
†These authors contributed equally to this work.

As a proof of principle of gene-based therapeutics for cancer, we designed recombinant adeno-associated virus (rAAV) vectors to express a bispecific T cell engager. These proteins are typically composed of two different antibody single-chain variable fragments (scFv) connected by a linker [a bispecific tandem diabody (*1*)] and transiently join T cells to target cells, promoting T cell activation and target cell apoptosis. The most advanced of these agents is blinatumomab, composed of an anti-CD19 scFv linked to an anti-CD3 scFv, which is currently Food and Drug Administration (FDA)–approved for CD19$^+$ B cell acute lymphoblastic leukemia (ALL) in children and adults who have either relapsed or refractory disease or who have minimal residual disease after first or second remission. The short half-life of blinatumomab [~2.1 hours; (*2*)] necessitates its continuous intravenous infusion over a period of 2 to 6 months (with intermittent breaks). As a consequence, the full utility of this therapeutic to subject cancer cells to consistent, long-term pressure has not been realized.

We created an rAAV with a human codon-optimized transgene encoding a signal peptide followed by the amino acid sequence of blinatumomab, which we term CD19 TransJoin, named for expression of a transgene that joins two cells together. We refer to the secreted protein product produced by the virus as an anti-CD19–anti-CD3 (αCD19-αCD3) "dimert." In addition to only requiring a single dose, our system also enables prolonged pressure on the target tumor cell, resulting in therapeutic expression for more than 1 year, a feature thought to be important for long-term cures elicited by chimeric antigen receptor (CAR) T cell approaches. Unlike CAR-T cells, however, TransJoin is an off-the-shelf solution, circumventing cumbersome manufacturing challenges inherent to CAR-T therapy.

To address clinical scenarios that require only short-term expression or recurring, intermittent expression of a therapeutic, we also developed a companion AAV construct termed TransSkip, in which we inserted two introns flanking a defective exon into the transgene coding sequence. Thus, constitutive exon inclusion in untreated samples renders the transgene nonfunctional. Upon administration

of a morpholino complementary to the 3′ exon splice site, the exon is skipped, resulting in alternate splicing that restores full-length transgene expression. TransSkip, therefore, represents an inducible gene therapy modality.

## RESULTS

### TransJoin development

We created and tested AAV viral vectors using the known strong CAG promoter (1.7 kb) designed to express the amino acid sequence of blinatumomab with human optimized codons. Because efficient protein secretion into the bloodstream is of paramount importance to our strategy, we appended the computationally designed secrecon (*3*) signal peptide to the N terminus of our transgene. We initially tested it with or without extra C terminus alanines (Fig. 1A) as their inclusion can markedly alter secretion depending on the expressed protein (*3*). We found that media from 293T cells transfected with each of the three secrecon-containing AAV plasmids competed with anti-CD3ε for binding to Jurkat T cells, whereas media from cells transfected with a plasmid lacking a signal peptide sequence showed no competition relative to controls (Fig. 1B). We selected the Sec1A construct for further studies and confirmed that media from Sec1A-transfected cells also competed with anti-CD19 for binding to Raji lymphoma cells, both in a dose-dependent fashion (Fig. 1C).

To demonstrate in vivo utility, we administered a single intravenous injection of the Sec1A construct packaged into AAV8 (AAV8-CAG193) at three different doses to mice engrafted with humanized immune systems (*4*). We observed rapid ablation of B cells with concomitant, albeit variable, stimulation of $CD4^+$ and $CD8^+$ T cells (Fig. 1D), consistent with human data using blinatumomab (*5*). B cell ablation was persistent at all late time points we tested, up to 42 weeks in the mouse given the highest virus dose. We administered AAV8-CAG193 to a single humanized mouse bearing a ~300-$mm^3$ flank Raji lymphoma and observed growth over the first 3 weeks followed by slow shrinkage, reaching a complete response by day 64 (Fig. 1E). In contrast, the AAV8–green fluorescent protein (GFP)–treated control mouse reached end point by 32 days. We expanded these studies to a similar model in which Raji-Luc/GFP lymphoma cells were introduced into immunodeficient mice that are also given an intravenous infusion of human peripheral blood mononuclear cells (huPBMCs; Fig. 1F). In this model, a single virus injection was effective at eliminating the tumor as measured by in vivo bioluminescence, caliper measurements, and animal survival (Fig. 1, G to I). We euthanized surviving animals after day 42 to determine vector biodistribution. Quantitative real-time polymerase chain reaction (PCR) analysis of AAV genomes at necropsy showed the vector widely distributed as expected but predominantly in the heart, liver, and muscle, with essentially none in the brain and spleen (Fig. 1J). We also determined that the weight loss we observed in treated animals after day 30 was consistent with graft-versus-host disease resulting from injecting human immune cells into a mouse host, as histopathology showed extensive perivascular histiocytic infiltrates in the liver, lung, and colon characteristic of this model (*6*). To confirm that there was no toxicity because of treatment, we repeated the experiment and euthanized all four groups (huPBMC alone, AAV8-CAG193, AAV8-GFP + huPBMCs, and AAV8-CAG193 + huPBMCs) at day 21 and measured serum chemistries, mouse cytokines/chemokines, human T cells, and mouse immune cells (Fig. 2). We did not find any differences between the groups for any parameters except human T cells, which were increased in mice given AAV8-CAG193 as expected with T cell activation against tumor cells.

To determine the efficacy of treatment in a more established tumor, we performed a similar experiment but waited longer (10 days) following tumor cell implantation to increase the tumor burden before providing huPBMCs (Fig. 3A). Again, all control groups required euthanasia because of tumor burden by 4 weeks (Fig. 3, B and C). In the treatment group (CAG193 + huPBMCs), tumors continued to progress for several weeks with 1 of 10 mice requiring euthanasia because of progression. Tumors reaching as large as 1300 $mm^3$ at week 4 slowly and consistently regressed over the following 8 weeks. Over that time period, one mouse was lost to anesthesia and three mice required euthanasia because of weight loss from graft-versus-host disease. Regardless, the overall survival was significantly extended by treatment (Fig. 3D).

We also created and tested a construct using a shorter promoter, EFS [232 base pairs (bp)], because AAV capacity is generally limited to <4.7 kb. A weaker promoter might also exhibit decreased genotoxicity from activation of adjacent genes during rare host cell insertion events (*7*). In this revised construct, we included a downstream woodchuck hepatitis virus posttranscriptional regulatory element (WPRE) RNA stability element (*8*) in an effort to maximize transgene expression from a less robust promoter (Fig. 4A). We also switched the AAV serotype to rhesus (rh)74, given our intention to use rh74 in the clinic because some studies suggest a lower prevalence of preexisting antibodies to rh74 than other serotypes in humans. As seen with our earlier construct, a single virus injection was effective at eliminating tumor as measured by in vivo bioluminescence, caliper measurements, and animal survival (Fig. 4, B to F), with serum αCD19-αCD3 dimert levels persistent at time of sacrifice and within the expected therapeutic range for blinatumomab (Fig. 4E). To determine an early pharmacokinetic time course of expression that adhered to Institutional Animal Care and Use Committee (IACUC) regulations, we measured αCD19-αCD3 dimert serum levels as "blinatumomab equivalents" (interpolated from a standard curve developed using blinatumomab) taken from seven mice using a different mouse each day of the week, enabling us to generate a pharmacokinetic profile (Fig. 4G). Serum levels slowly increased following virus infusion and reached a steady state by 2 weeks. Furthermore, to evaluate the relationship of dose to serum levels and long-term expression, we performed a separate experiment in which we injected mice of both sexes with three different doses and observed a dose-dependent effect on long-term steady-state levels (Fig. 4H). Levels were relatively constant for at least 1 year, and animals showed no signs of toxicity with normal weight gains similar to control animals.

### TransSkip development

In addition to constitutive expression afforded by the TransJoin design, we also sought to create a controllable version that might be suitable for scenarios requiring only short-term but repeated use or perhaps in the event of side effects. Toward this end, we based our strategy on principles of exon splicing regulation. We reverse-engineered a purposefully faulty exon into the coding sequence that could be excluded (skipped) using an antisense morpholino. Because on-target exon skipping in a normal cellular gene might be harmful, we decided to use an intron derived from the *KRAS* gene [which is among the most commonly activated oncogenes in human cancer (*9*)]

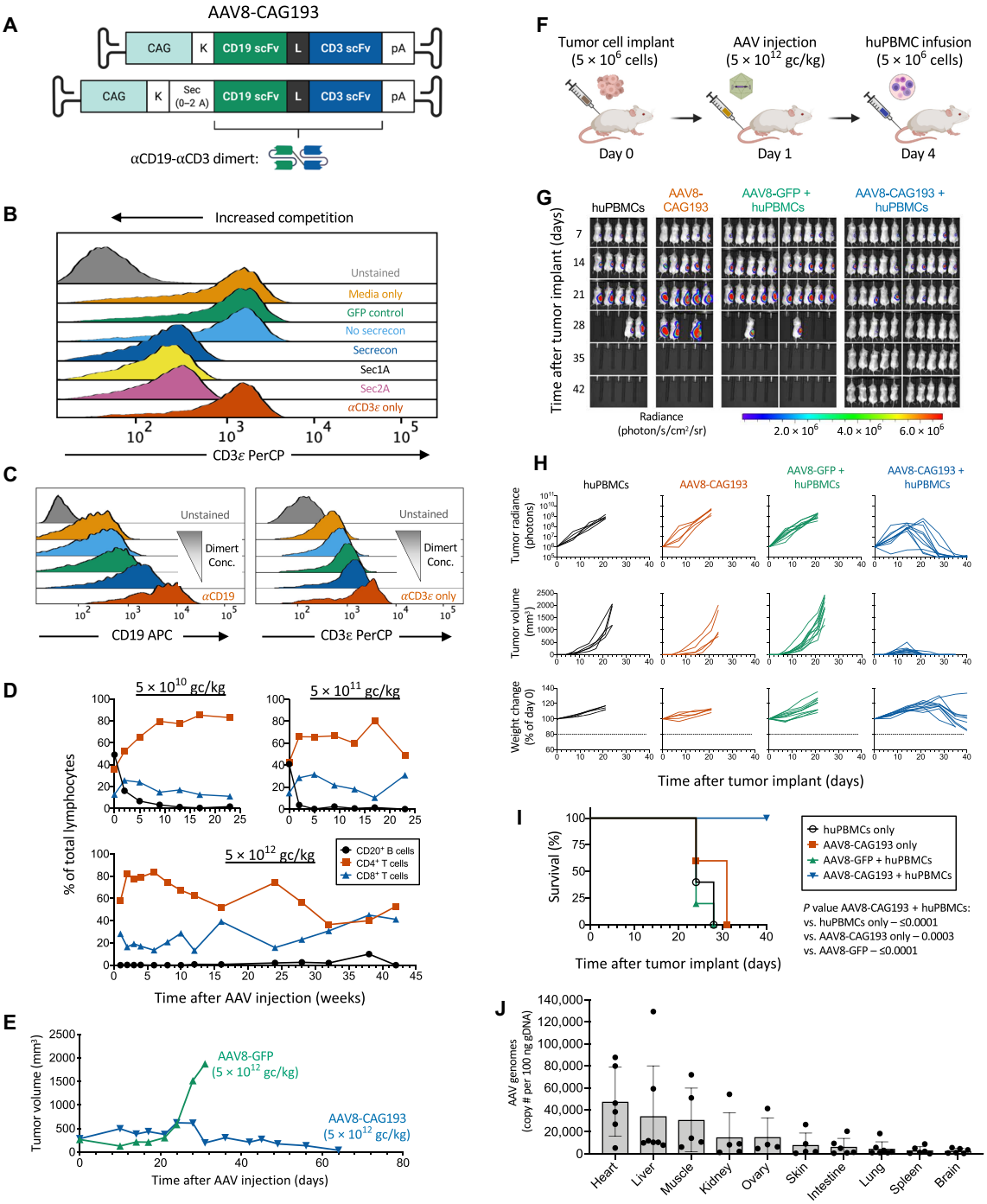


**Fig. 1. Construction and verification of an αCD19-αCD3 dimert construct for AAV delivery.** (**A**) Schematics of αCD19-αCD3 dimert–expressing plasmids. CAG, cytomegalovirus (CMV) early enhancer/chicken β-actin promoter; K, Kozak sequence; Sec, secrecon signal peptide with 0 to 2 alanine spacers; pA, polyadenylation site. The dimert protein is composed of single-chain antibodies for CD19 (clone HD37) and CD3 (clone L2K-07) joined by a peptide linker (L). (**B**) Flow cytometry histograms of Jurkat T cells following exposure to media containing αCD19-αCD3 dimerts. Secreted dimerts compete with labeled CD3ε antibody for access to the Jurkat cells, reflected by a signal shift on the *x* axis. (**C**) Competitive binding assays demonstrating a dose-response effect of the Secrecon$^{+1}$ alanine (Sec1A) αCD19-αCD3 dimert in binding to CD19 and CD3ε on Raji and Jurkat cells, respectively. APC, allophycocyanin. (**D**) Impact of AAV8-αCD19-αCD3 (AAV8-CAG193) administration on CD20$^+$ B cell and CD4$^+$ and CD8$^+$ T cell populations in humanized mice. Each graph represents a single mouse. (**E**) AAV8-CAG193 administration ($5 \times 10^{12}$ gc/kg) resulted in tumor clearance in a Raji lymphoma–bearing humanized mouse. (**F**) Treatment regimen for double-blinded AAV8-CAG193 efficacy study. (**G**) Bioluminescent images of the mice over time. (**H**) Top row: Individual tumor bioluminescent values over time. Middle row: Tumor volumes calculated by caliper measurements. Bottom row: Individual mouse weight changes, presented as percent change from initial weight. (**I**) Kaplan-Meier survival curve. Statistical significance was determined using the log-rank test [$n = 5$ for human peripheral blood mononuclear cell (huPBMC) and AAV8-CAG193 only mice, $n = 10$ for AAV8–green fluorescent protein (GFP) + huPBMC and AAV8-CAG193 + huPBMC mice]. (**J**) Biodistribution of AAV8-CAG193 in mouse tissues. Error bars represent SD ($n = 4$ to 7 per tissue).

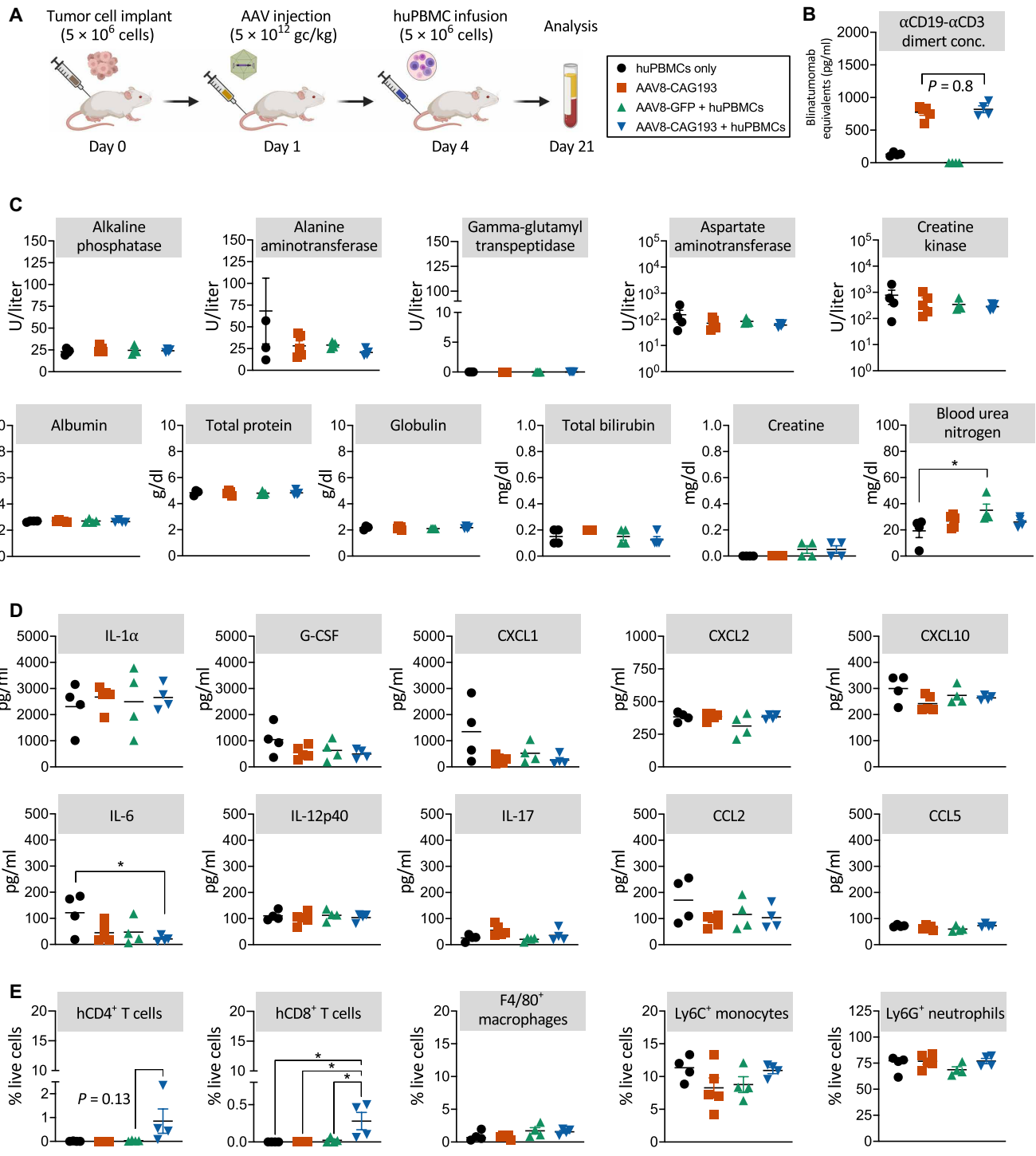


**Fig. 2. Preclinical evaluation of potential toxicity in NSGS mice bearing Raji-Luc/GFP tumors treated with AAV8-CAG193 and huPBMCs.** (**A**) Graphical representation of the experiment timeline, mirroring the efficacy study presented in Fig. 1. The mice were euthanized on day 21 after tumor implantation for analyses. (**B**) Serum concentration of αCD19-α CD3 dimert present in each experimental group at the time of sacrifice. Dimert quantification was performed using a T cell activation assay and interpolated from a blinatumomab standard curve. (**C**) Serum chemistry profiles of the mice in each experimental group as determined by the AU680 Chemistry System (Beckman Coulter). Values from the AAV-treated groups were generally in line with the control huPBMC group apart from slightly elevated levels of blood urea nitrogen in the AAV-GFP group. (**D**) Enzyme-linked immunosorbent assay analyses of murine cytokine and chemokine levels in the serum at the time of sacrifice. (**E**) Flow analysis of peripheral blood samples from each mouse at the time of sacrifice and examining the levels of human T cells and murine macrophage, monocyte, and neutrophil cell populations. Statistical significance was assessed with one-way analysis of variance. *$P \leq 0.05$. IL-1α, interleukin-1α; G-CSF, granulocyte colony-stimulating factor.

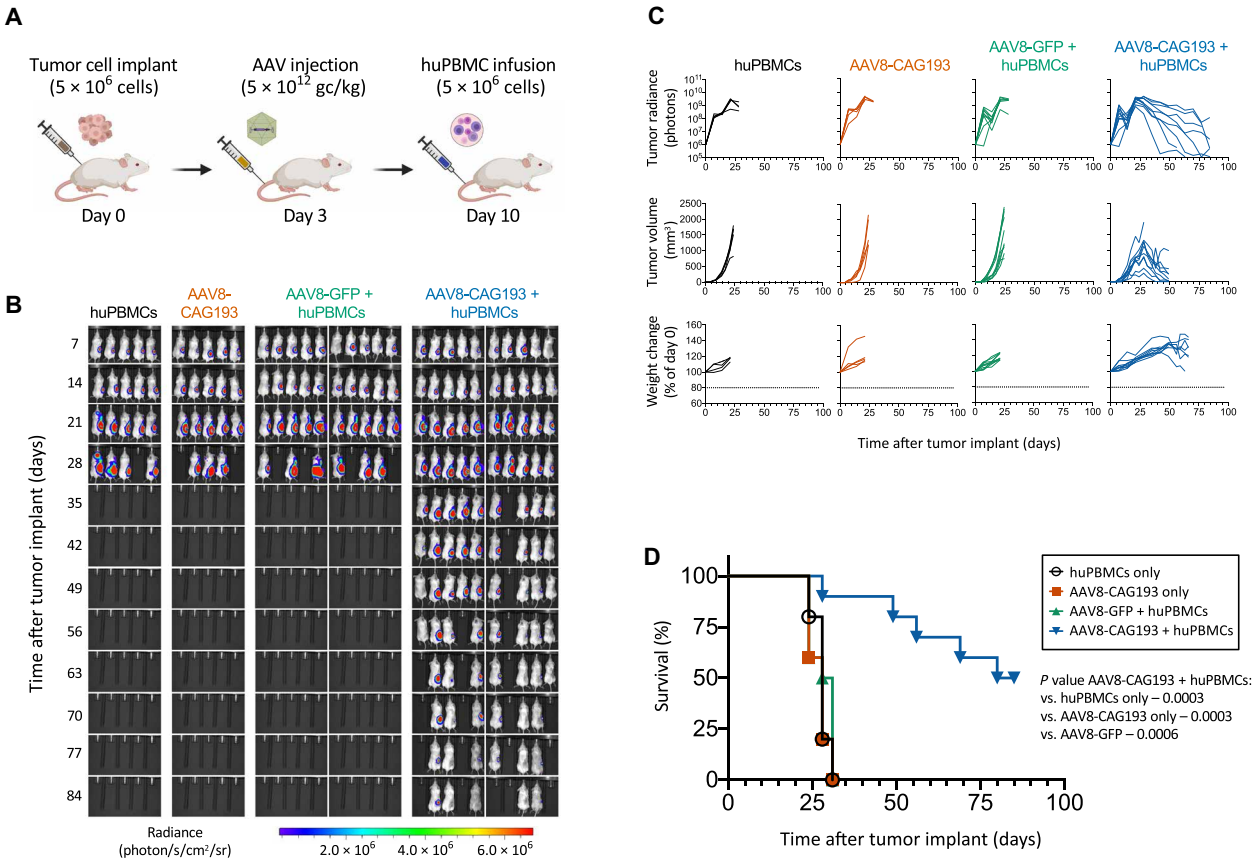


**Fig. 3. Preclinical evaluation of AAV8-CAG193 in NSGS mice bearing more established Raji-Luc/GFP tumors.** (**A**) Graphical representation of alternative treatment regimen enabling larger Burkitt's lymphoma tumors before therapy. (**B**) Bioluminescent images of tumors in each treatment group. (**C**) Individual tumor bioluminescent values recorded for each mouse are shown in the top row of panels. Tumor volumes calculated by caliper measurements are shown in the middle row, and weight changes over time are displayed in the bottom row, presented as a percent change of each individual mouse's initial weight. (**D**) Kaplan-Meier survival curve. Statistical significance was determined using the log-rank test ($n = 5$ for HuPBMC and AAV8-CAG193 only mice and $n = 10$ for AAV8-GFP + HuPBMC and AAV8-CAG193 + HuPBMC mice).

as its morpholino-induced depletion might also prove to be therapeutically beneficial. To achieve a regulatable splicing cassette exon in our construct, we inserted into the coding sequence of the anti-CD19 scFv arm of the transgene a modified *KRAS* Exon 1, flanked by 150-bp introns. The 5′ intron was derived from intron sequences upstream of the native *KRAS* Exon 1 by linking the 5′ 75 bp to its 3′ 75 bp (Fig. 5A). Similarly, the 3′ flanking intron was derived from the intron downstream of the native *KRAS* Exon 1. These truncated "mini-introns," which were used because of size constraints, nonetheless house the native splice sites and regulatory regions required for splicing.

We chose the second exon (Exon 1) of *KRAS* because it contains the *KRAS* transcriptional start site and, if excluded, would be expected to reduce expression of full-length Kras protein. We mutated Exon 1 within the TransSkip construct to contain stop codons in all three reading frames to ensure a nonfunctional transgene when included in the transcript. We refer to this intron-exon-intron derivative as the *KRAS* Exon 1–mutated (KM) cassette. We hypothesized that the introduction of a morpholino [termed *KRAS* TransSkip (KTS)] designed to skip the exon based on interference with the 3′ exon spliceosome binding sites would induce expression of the therapeutic transgene in virus-transduced cells and simultaneously down-regulate Kras expression in cancer cells (Fig. 5A).

We identified transgene coding sequences where the exonic portion of a consensus splice donor sequence (AAG or CAG) were fortuitously located adjacent to the exonic portion of a consensus splice acceptor sequence (GG or GT) so that an insert placed there, when spliced out, would yield the native sequence. We inserted the KM cassette in the most 5′ site option of the potential splice donor/acceptor sequence junction to disrupt the coding sequence as early as possible during translation (Fig. 5B). As measured by reverse transcription PCR (RT-PCR) of mRNA from plasmid-transfected 293T cells, this initial configuration (KM1) showed mostly transcripts containing all three exons with a substantial dose-dependent increase in exon skipping following exposure to the KTS morpholino with its Endoporter carrier but not an inverted (KTSinvert) morpholino control (Fig. 5C).

With the KM1 construct, we noted detectable levels of skipped mRNA in the mock-treated samples. Consistent with this skipped mRNA, we detected functional protein expression (using the antibody competition assay from Fig. 1C), nearly fully competing out anti-CD3ε binding. To further optimize the construct to reduce the skipped mRNA expression in the absence of morpholino, we created and tested two other variants (KM2 and KM3) with base pair substitutions in the polypyrimidine U2 auxiliary factor splicing factor binding site at the 3′ splice site of the upstream intron. The idea was

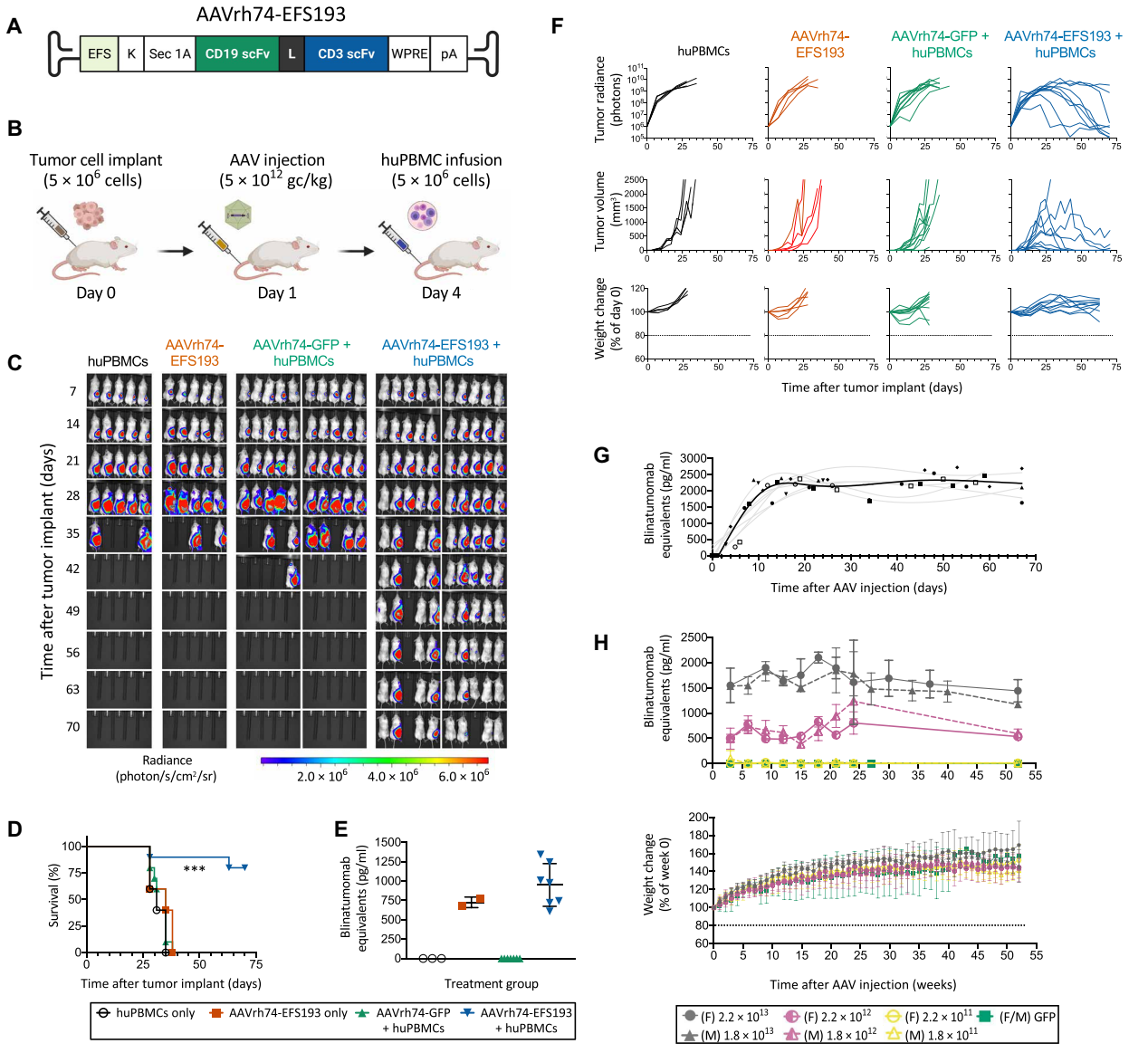


**Fig. 4. AAV gene therapy using an EFS promoter–driven αCD19-αCD3 dimert reduces tumor burden and significantly increases survival in a mouse xenograft model of Burkitt's lymphoma.** (**A**) Construct map of AAVrh74-EFS193. The αCD19-αCD3 dimert itself is identical in sequence to that described in Fig. 1A. EFS, promoter from elongation factor 1α (short form); WPRE, woodchuck hepatitis virus posttranscriptional regulatory element. (**B**) Nod-scid gamma-SGM3 (NSGS) mice were implanted subcutaneously with 5 × $10^6$ Raji-Luc/GFP lymphoma cells and injected with AAV (5 × $10^{12}$ gc/kg) the following day. (**C**) Bioluminescent images of NSGS mice bearing Raji-Luc/GFP lymphoma tumors. (**D**) Kaplan-Meier survival curve. Statistical significance was determined using the log-rank test ($n = 5$ for huPBMC and AAVrh74-EFS193 only mice and $n = 10$ for AAVrh74-GFP + huPBMC and AAVrh74-EFS193 + huPBMC mice). (**E**) Serum concentration of αCD19-αCD3 dimert at the time of each mouse's sacrifice. Dimert quantification was performed using a T cell activation assay and interpolated from a blinatumomab standard curve. (**F**) Associated values for tumor radiance, tumor volume, and mouse weights over the course of the experiment. (**G**) Production of EFS-driven αCD19-αCD3 dimert in NSGS mice over time. Dimert quantification was performed using a T cell activation assay and interpolated from a blinatumomab standard curve. Each data point represents a serum sample from an individual mouse. (**H**) Top: Comparison of EFS-driven αCD19-αCD3 dimert production in female (F) and male (M) NSGS mice over time at different dose levels. The numbers in the key correspond to the AAV dose in gc/kg. GFP denotes control mice injected with AAVrh74-GFP (2.2 × $10^{12}$ gc/kg for female and 1.8 × $10^{12}$ gc/kg for male). Bottom: Corresponding mouse weights for the longitudinal dimert quantification assay. Weights are presented as the average percent change for each treatment group ($n = 3$ to 5 for AAVrh74-EFS193 treatment groups and $n = 1$ to 2 for AAVrh74-GFP controls).

to increase inclusion of the exon in the absence of morpholino yet retain susceptibility to exon skipping upon morpholino administration. Levels of the exon-excluded mRNA transcript (mock-treated lanes) were essentially nonexistent in these two variant constructs, and no protein was detected by the anti-CD3 binding competition assay. Despite this absence, the addition of morpholino led to exon skipping in both the KM2 and KM3 constructs as evidenced by increased competition for anti-CD3ε binding in the associated flow histograms.

To test the utility of the TransSkip system in vivo, we administered either the constitutive CD19 TransJoin (AAV8-EFS193) or the KM2 version of CD19 TransSkip (AAV8-EFS-KM2-193) to immunodeficient mice and followed serum levels of the αCD19-αCD3 dimert

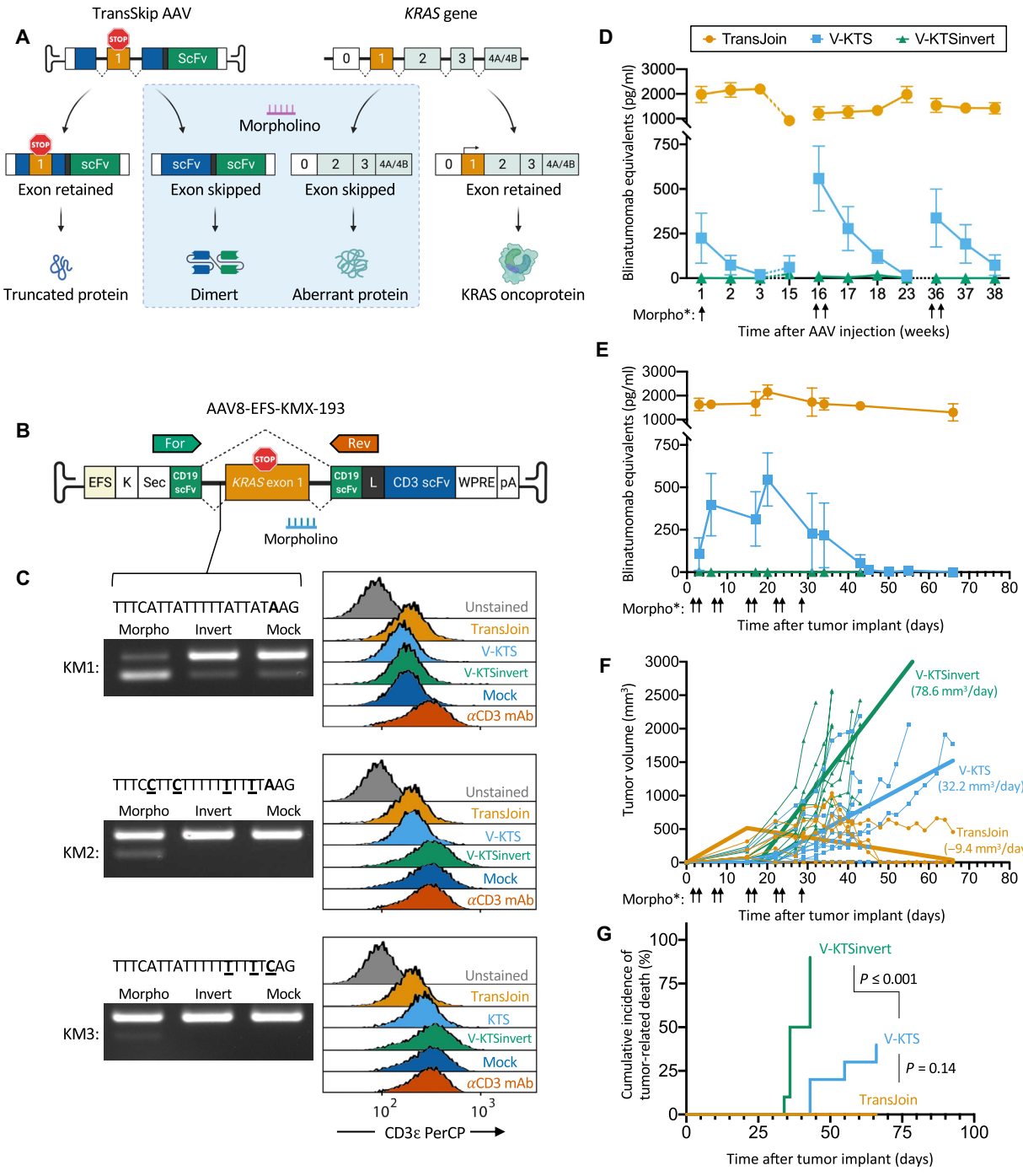


**Fig. 5. Inducible dimert technology (TransSkip).** (**A**) The dimert coding sequence is interrupted by a mutated version of Exon 1 (stop codons in all reading frames) and flanking intronic sequences derived from the human *KRAS* gene. A functional dimert mRNA is expressed when a complementary morpholino binds to the exon-intron junction and induces exon skipping. Because the wild-type exon contains the *KRAS* transcriptional start site, the morpholino was designed to also down-regulate endogenous KRAS expression. (**B**) Generalized construct map of a αCD19-αCD3 TransSkip dimert. The forward ("For") and reverse ("Rev") RT-PCR primers are shown by arrows. (**C**) Three constructs with different U2AF splicing factor binding site sequences were evaluated for exon skipping after morpholino administration, where a lower band indicates the skipped mRNA (coding for an intact dimert). Flow histograms show the results of competitive binding assays for access to CD3ε on Jurkat T cells. mAb, monoclonal antibody. (**D**) Production of αCD19-αCD3 dimert in NSGS mice injected with $5 \times 10^{12}$ gc/kg AAV8-EFS193 (TransJoin) or AAV8-EFS-KM2-193 (TransSkip) with functional (V-KTS) or inverted vivo-morpholino (V-KTSinvert), both administered at time points shown by arrows. Error bars represent SD. (**E**) Production of αCD19-αCD3 dimert in Raji-Luc/GFP tumor–bearing NSGS mice. The experimental design is identical to Fig. 1F apart from the administration of morpholinos. (**F**) Individual tumor volumes for each treatment cohort over time were plotted against predicted growth trend (thick lines) as determined by mixed-effects modeling. Values in parentheses indicate average tumor growth rate per day. (**G**) Plot of cumulative incidence of death related to tumor burden for each treatment group. Statistical significance was assessed using Gray's test.

over time. At periodic intervals, we administered either a single intravenous dose (week 1) or two intravenous doses of the KTS morpholino (Vivo-KTS) on two consecutive days (weeks 16 and 36) to the CD19 TransSkip–treated mice; at those time points, we gave an inverted morpholino (Vivo-KTSinvert) to a separate cohort of CD19 TransSkip–treated mice to serve as a control. As anticipated, we observed robust expression of αCD19-αCD3 in the sera of CD19 TransJoin–treated mice and no detectable αCD19-αCD3 dimert levels in CD19 TransSkip–treated mice given Vivo-KTSinvert throughout the course of the experiment (Fig. 5D). In contrast, mice given Vivo-KTS produced αCD19-αCD3 dimert within 1 day of its administration, which then slowly faded back to uninduced levels over a 2- to 3-week period. We were able to reinduce expression each time we gave Vivo-KTS over the course of nearly a year. These data show in vivo proof of principle for using exon skipping to intermittently and repeatedly activate therapeutic protein expression from an AAV construct. We also administered repeated doses of Vivo-KTS over 5 weeks, demonstrating that we could achieve sustained expression over a longer period of time (Fig. 5E). Although not as high as levels from the constitutive TransJoin construct, the levels were sufficient to elicit a modest therapeutic effect as seen by slower tumor growth (Fig. 5F) and fewer mice dying from tumor burden (Fig. 5G) compared with those treated with Vivo-KTSinvert.

### OncoSkip specificity

Last, we sought to determine whether KTS was effective at excluding the native *KRAS* Exon 1 in the cellular genome and decreasing Kras protein, a process we term OncoSkip. When incubated with tumor cells in culture, KTS resulted in skipping of the native *KRAS* gene in a dose-dependent fashion in three different cancer cell lines and primary human hepatocytes (Fig. 6A), but we did not observe a decrease of Kras protein on Western blots (Fig. 6B). To confirm and better quantify skipped mRNA, we quantified the transcript isoforms using Single-Molecule Real-Time (SMRT) Iso-Seq in H441 lung cancer cells treated with KTS, KTSinvert, or Endoporter alone (Fig. 6C). While we detected various isoforms, none lacked *KRAS* Exon 1 in the two control groups, whereas *KRAS* Exon 1 was missing from 37% (39 of 105) of transcripts in KTS-treated cells. We were not able to identify any off-target skipping of other genes when we searched for potential homologous sequences in the genome and compared transcript isoforms among the three treatment groups.

## DISCUSSION

Systemic gene therapy using AAV is under intense study to treat rare, single-gene diseases such as hemophilia and muscular dystrophy (*10*) and has been FDA-approved to treat spinal muscular atrophy. Here, we report a previously undescribed method to use the same platform to achieve sustained expression of a therapeutic protein into the bloodstream following a single intravenous injection. As proof of concept, we expressed a blinatumomab-mimic (αCD19-αCD3 dimert), cleaved from a propeptide and secreted into the bloodstream of mice from different constructs (CD19 TransJoin), for at least 1 year without toxicity. A single administration was sufficient to treat mice harboring a $CD19^+$ flank lymphoma. We did not observe effects on tumor shrinkage until 2 to 3 weeks following injection, consistent with the delay of approximately 2 weeks to reach steady-state pharmacokinetics. In some animals, we observed relatively large tumors (up to ~1500 $mm^3$) completely resolve. Reductions in tumor volumes occurred slowly, generally over weeks to months, highlighting the need for consistent, long-term therapeutic expression as provided by our approach. In addition to $CD19^+$ malignancies, due to its long-term persistence, CD19 TransJoin therapy also might be useful to treat chronic conditions with B cell–mediated pathophysiology including certain autoimmune disorders such as multiple sclerosis (*11*). The single-dose concept might be especially useful for patients in underserved populations who currently need to travel long distances repeatedly for treatment.

To address scenarios requiring short-term or intermittent expression, we also created an inducible expression system by engineering into the transgene a defunct exon that can be excluded by an exogenous morpholino. Insertion of the intron-exon-intron cassette was effective at eliminating detectable expression of the transgene in the blood of mice following systemic injection of $5 \times 10^{12}$ genome copies per kilogram. Systemic administration of the cognate morpholino was repeatedly effective at inducing expression of blinatumomab to over 500 pg/ml equivalents. Following each induction, we observed a slow fade in expression over 10 to 14 days. The duration of the expression is likely the result of the tissue-resident time of the morpholino and the mRNA half-life. We also showed that we could sustain expression with repeated injections. Although the levels were only about 25% of those achieved with the constitutively expressed vector, we did achieve sufficient expression to elicit a therapeutic effect. In addition to treating intermittent disease flares, the system could be used where a single transient expression is desirable, such as expression of Cas9 for gene editing to possibly minimize off-target effects (*12*) and to reduce immune-mediated destruction of transduced cells (*13*), either in vivo or ex vivo. Given that splice-modulating oligonucleotides have been FDA-approved for multiple genetic disorders (*14*), this approach should be clinically translatable.

Our strategy solves the short half-life challenge of small diabodies such as blinatumomab, which is 2.11 hours in humans (*2*), necessitating continuous infusion, frequent syringe replenishments, and poses infection risks that hamper its long-term use. Short-term, blinatumomab is highly effective and is FDA-approved for both pediatric and adult patients with relapsed ALL or who have minimal residual disease. In the pivotal TOWER study, however, blinatumomab patients were only given an average of two cycles (4 weeks on, 2 weeks off; ranging from 1 to 9) (*15*), so they might not have received the full benefit that would likely result from longer exposure. Similarly, in a single-arm study of up to four cycles of blinatumomab given to patients with minimal residual disease, 79.6% achieved a complete response after two cycles (*16*). Unfortunately, 34.5% eventually relapsed, suggesting that they might have benefited from longer exposure to the therapeutic agent.

Blinatumomab also shows efficacy in patients with $CD19^+$ non-Hodgkin's lymphomas (*5*, *17*). Pharmacodynamic modeling suggested that efficacy is dependent on exposure levels and duration with steady-state levels >1830 pg/ml being desirable for anti-lymphoma activity, which is higher than levels found in patients with ALL at the recommended dose of 28 μg/day (731 ± 444 pg/ml) (*18*). These levels were readily achievable in our mouse studies. The data also suggested that prolonged exposures are required for shrinkage of lymphoma masses, reducing in half every 4 weeks (i.e., 12 weeks for 87.5% reduction). Most patients, however, received only 4 weeks of therapy, with others going only out to 9 weeks maximum. Thus, the utility of even longer-term therapy with blinatumomab for lymphoma was likely unrealized.

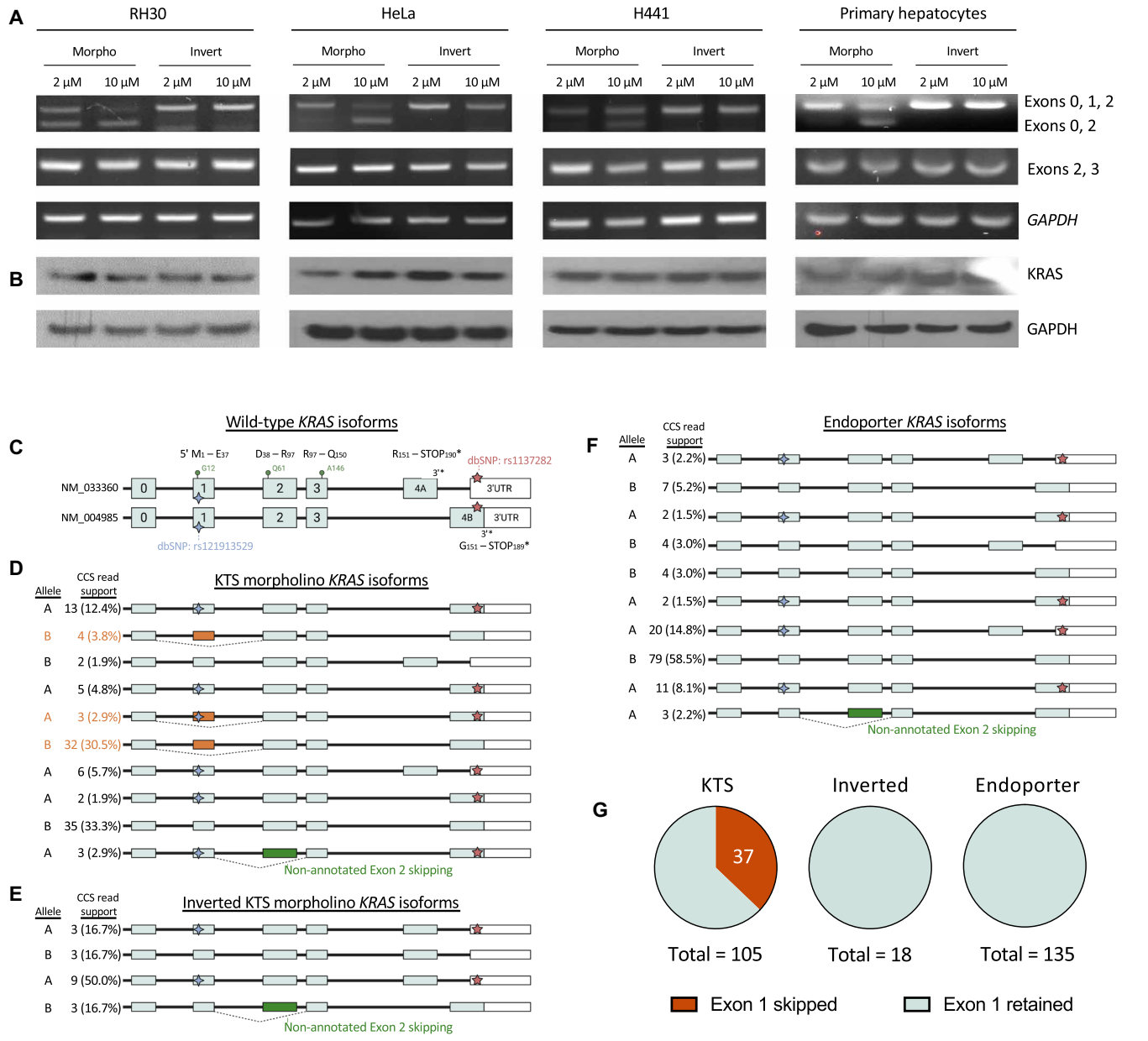


**Fig. 6. In vitro verification of *KRAS* Exon 1 skipping in cancer cells.** (**A**) RT-PCR of treated RH30 rhabdomyosarcoma, HeLa cervical cancer cells, H441 lung adenocarcinoma cells, and primary human hepatocytes following exposure to KTS morpholino or its inverted control. The upper 307-bp band indicates the presence of Exon 1 in the PCR amplicon, whereas the lower 185-bp PCR amplicon indicates exon skipping. We observed a dose-dependent induction of *KRAS* Exon 1 skipping following treatment with the morpholino, while *KRAS* Exon 2/3 and *GAPDH* housekeeping controls were not affected. (**B**) Immunoblots of KRAS and glyceraldehyde-3-phosphate dehydrogenase (GAPDH) protein levels for the cell lines in (A). (**C**) *KRAS* expressed isoforms identified by PacBio Iso-Seq. 3′UTR, 3′ untranslated region. (**D** to **F**) *KRAS* isoforms detected in H441 cells exposed to KTS morpholino, inverted morpholino, or endoporter control. Isoforms displaying Exon 1 skipping are highlighted. Allele phasing by single nucleotide polymorphism database (dbSNP) represented by A (dbSNP containing) or B (lack of dbSNP) allele designation. (**G**) Percentage of circular consensus sequencing (CCS) reads that displayed *KRAS* Exon 1 skipping for each treatment group.

CAR-T cells directed at CD19 have also been a breakthrough for B cell leukemias and lymphomas (*19*), and their long-term persistence is thought to be an important feature of their success. That said, CAR-T technology requires conditioning chemotherapy, and manufacturing remains a substantial and cumbersome challenge as cells are prepared from each individual patient and may have poor yield, inefficient gene transduction, reduced function, and poor persistence resulting in relapsed disease (*20*). TransJoin is an off-the-shelf alternative approach for achieving long-term redirection of T cells to target cells without these issues. While allogeneic CAR-T cells also promise to circumvent these challenges, issues of graft-versus-host disease and clearance by host immunity will need to be solved for them to be successful (*21*).

Several other gene-based approaches have been tested to express diabodies. In a study using electroporation of plasmid DNA into muscle, a bispecific T cell engaging diabody against human epidermal

growth factor receptor 2 (HER2) showed antitumor efficacy in a model of $HER2^+$ ovarian cancer (*22*). Expression waned steadily after the first few weeks, however, and was extinguished at ~4 months. The local delivery also remains a challenge and is unlikely to yield high systemic levels. Others have incorporated transgenes into oncolytic viruses that add to their antitumor efficacy (*23*, *24*), but these vectors result in only short-term expression because the viruses kill the cells they infect. Transgenes have also been tested in adoptive cell therapies such as CAR-T cells (*25*), although these approaches are not off-the-shelf solutions in contrast to AAV gene transfer.

Potential toxicities from TransJoin could arise from both the vector and the transgene. Although we did not observe any safety signals in our short-term or long-term mouse studies, concerns have been raised in neuromuscular AAV9 (but not AAVrh74) trials regarding antiviral immune reactions including complement activation and liver toxicity (*26*). Whereas high vector doses [$10^{14}$ vector genomes (vg)/kg] are required to reach a high proportion of nerve or muscle cells in the neuromuscular disorders, only a fraction of liver (or other) cells need to be transduced for successful TransJoin therapy (similar to hemophilia gene therapy). Thus, consistent with our mouse data and with human hemophilia studies, we expect human dosing to only require in the range of $10^{12}$ vg/kg, reducing the likelihood of vector-mediated toxicities.

Regarding toxicities from the transgene, we expect expression of αCD19-αCD3 to pose some risk of cytokine release syndrome (CRS) and immune effector cell–associated neurotoxicity syndrome (ICANS), similar to other CD19-targeted immunotherapies including both blinatumomab and CAR-T. In the TOWER study of blinatumomab, 5% of patients experienced grade 3 or higher CRS and 9% experienced ICANS (*27*), most of which occurred in the first few cycles, similar to findings in another study (*16*). Because stepwise dosing showed lower cytokine levels (*5*), the recommendation for administration of blinatumomab is to begin with one-third of the dose for the first week and then escalate to full dose. The slow accumulation of serum levels over about 2 weeks that we observed using the AAV platform should similarly minimize the risk of CRS early during therapy. Whereas blinatumomab infusions can be discontinued, however, with CD19 TransJoin, we will need to rely on anti–interleukin-6 therapies for CRS and supportive care options to manage ICANS, similar to what is done with CAR-T patients who also do not have an "off switch."

AAV has been previously tested as a platform to express anti-infection antibodies such as to treat HIV (*28*). One limitation that arose in nonhuman primate studies is the development of an immune reaction against the transgene product, so-called antidrug antibodies (ADA). We do not expect ADA to be a limitation for CD19 TransJoin as <1% of patients treated with blinatumomab develop ADA (*2*), likely because it depletes B cells required for neo-antibody production. We expect some patients treated with CD19 TransJoin to require restoration of their humoral immunity with monthly infusions of intravenous immune globulin, as is the case for those treated with CD19-directed CAR-T therapy (*29*).

To achieve intermittent expression using TransSkip, we chose to use the sequence of the oncogene *KRAS* as the source of our artificial exon in the event it might simultaneously have antitumor activity. While we were able to demonstrate a moderate down-regulation of total *KRAS* mRNA, it did not appear to be sufficient to affect Kras protein levels. It may yet be possible to realize this potential benefit as morpholino technology improves, for example, with the use of stereoisomer (*30*) oligonucleotides or peptide phosphorodiamidate morpholino oligonucleotides (*31*), both of which have shown improved efficiency. With more efficient skipping, there could be the possibility of on-target, off-tumor toxicities, so the normal gene used as a sequence for the TransSkip construct morpholino target would need to be chosen carefully. That said, we can envision paired TransSkip/OncoSkip therapies in which the relevant oncogene driving a given tumor type is used to activate expression of a relevant therapeutic.

Tight control of transgene expression has long been sought for gene therapy applications. The most commonly used Tet-On/Off system used in the laboratory setting is limited in vivo by immune reactions to the bacterial proteins (*32*). More recently, an on-switch that, similar to our approach, avoids immunogenic regulatory proteins was described in an AAV transgene setting (*33*). The authors achieved constitutively low expression by incorporating a self-cleaving hammerhead ribozyme into the RNA transcript, which was counteracted by an antisense oligonucleotide resulting in transgene expression. The approach worked best following direct local administration of vector and antisense into muscle, but it was not effective with systemic administration.

In summary, we propose that long-term stable expression of biotherapeutics achievable by gene transfer can be leveraged to solve both the problem of fluctuating drug levels inherent to traditional administration routes and the cumbersome mechanics that accompany continuous intravenous infusions. For cancer, the advantage of our strategy is not only the single therapeutic administration rather than frequent clinic and hospital visits but also the prospect of long-term, consistent pressure on tumor cells that could address persistent micrometastatic disease that mediates relapse. We also developed a companion TransSkip on-switch that enables on-demand expression for scenarios in which only short-term or intermittent expression is preferable. These technologies conceptually open a broad new area of gene therapy to solve therapeutic challenges extending well beyond the correction of single-gene disorders.

## MATERIALS AND METHODS

### Cells and cell culture

The human cell lines Rh30 (CRL-2061; rhabdomyosarcoma), H441 (HTB-174; lung adenocarcinoma), Raji (CCL-86; Burkitt's lymphoma), HeLa (CCL-2; cervical adenocarcinoma), and 293T (CRL-3216; embryonic kidney) were all purchased from American Type Culture Collection (Manassas, VA). The Jurkat cell line (acute T cell leukemia) was a gift from R. Wang (Nationwide Children's Hospital, Columbus, OH). Rh30, H441, Raji, Raji-Luc, and Jurkat cells were all maintained in RPMI 1640 supplemented with 10% fetal bovine serum (FBS), penicillin (100 U/ml), and streptomycin (10 mg/ml). HeLa and 293T cells were all maintained in Dulbecco's modified Eagle medium supplemented with 10% FBS, penicillin (100 U/ml), and streptomycin (10 mg/ml). All cell lines were authenticated by short tandem repeat genotyping and confirmed negative for mycoplasma by IDEXX Bioanalytics (Columbia, MO).

Raji-Luc/GFP cells were created by transducing Raji lymphoma cells with a cytomegalovirus–driven Firefly luciferase–GFP lentivirus (Cellomics Technology, Halethorpe, MD) in accordance with the manufacturer's protocol. In short, Raji cells were incubated with lentivirus (multiplicity of infection = 1 lentiviral particle per Raji cell) and polybrene (2 μg/ml) for 24 hours. The transduced cells were

then pelleted and resuspended in fresh complete RPMI 1640 medium and allowed to grow for an additional 72 hours before the addition of puromycin (1 μg/ml) to aid in the selection of luciferase and GFP-positive cells. Raji-Luc/GFP cells were cultured and expanded in puromycin-containing media until passage number 5, whereupon frozen stocks were created to be used in this study.

Plateable cryo-preserved human hepatocytes (catalog no. HUCPG, Lonza Morristown, NJ USA) were thawed and transferred into 50 ml of warm thawing media (catalog no. MCHT50, Lonza) and spun down at 100*g* for 8 min. Cell pellets were resuspended in plating media (catalog no. MP100, Lonza) and plated on a collagen-coated six-well dish (catalog no. 354400 Corning Glendale, AZ, USA) at a concentration of $1 \times 10^6$ cells/ml. The plate was placed in 37°C/5% $CO_2$ incubator and shook every 15 min within an hour of incubation time. One hour later, the culture was replaced with fresh plating media and incubated for at least another 3 to 5 hours. Four to six hours after cell plating, the hepatocyte culture was replaced with maintenance media (catalog no. CC-3198, Lonza) for overnight incubation. The hepatocyte culture was replenished with fresh maintenance media daily during the assay period.

### Plasmid construction and AAV viral vector production

AAV viral vectors used to overexpress the αCD19-αCD3 or αCD3-αGD2 dimerts or the GFP control in our studies were constructed and packaged by Vector Builder into AAV8, and pAAV[Exp]-EFS > {Sec1A-319}:WPRE was also packaged into AAVrh74 by Andelyn Biosciences (Columbus, OH). The vector builder IDs are VB180911-1323bgt, VB180911-1324wfc, VB180911-1325nxj, VB180911-1327bav, VB190801-1073wgb, VB190812-1166hus, VB190513-1103mwk, VB190313-1119zah, VB190513-1105qjq, VB190513-1107xjy, VB190513-1108ykx, and VB190812-1168kyk, which can be used to retrieve detailed information about the vector on vectorbuilder.com. Table 1 denotes the experimental use for each AAV viral vector.

### Animals

Non-obese diabetic scid gamma (NSG)-SGM3 (013062) mice were procured from the Jackson Laboratory (Bar Harbor, ME) and bred in-house. $CD34^+$ humanized NSG-SGM3 mice were obtained from the Jackson Laboratory. NSG mice were obtained from Envigo (Indianapolis, IN). All animal experiments were approved by and performed in accordance with the regulations of the IACUC at Nationwide Children's Hospital.

**Table 1. AAV viral vectors.**

| Vector builder name | Figure |
|---|---|
| pAAV[Exp]-CAG > {CD3xCD19} | 1B |
| pAAV[Exp]-CAG > {sec0A-CD3xCD19} | 1B |
| pAAV[Exp]-CAG > {sec1A-CD3xCD19} | 1, B to J, and 2, A to E and 3, A to D |
| pAAV[Exp]-CAG > {sec2A-CD3xCD19} | 1B |
| pAAV[Exp]-EFS > {Sec1A-319}:WPRE | 4, A to H and 5, D to G |
| pAAV[Exp]-EFS > {Sec1A-319-K3}:WPRE | 5, C to G |
| pAAV[Exp]-CMV > EGFP | 1, B, E, G to I, 2, B to E and 3, B to D and 4, C to F, H |

### Depletion of B cells in $CD34^+$ humanized NSG-SGM3 mice

Sixteen- to 20 week-old female $CD34^+$ humanized NSG-SGM3 mice were administered with AAV8-CAG193 at $5 \times 10^{10}$, $5 \times 10^{11}$, and $5 \times 10^{12}$ gc/kg by tail vein injection. Systemic $CD20^+$ B cell population was assessed at $T = 0$ and then every 3 weeks by retro-orbital blood collection and flow cytometric analysis.

### Efficacy studies

All efficacy studies were double-blinded unless otherwise noted and involved no less than three laboratory personnel and one external person. The roles included an agent formulator, key master (blinder), gate keeper (external personnel), treatment administrator (blinded), data collector (blinded), data analyst (blinded), and post-analysis evaluator (unblinded).

For the early stage tumor model, $5 \times 10^6$ Raji-Luc/GFP cells were implanted on day 0 in the right flank of 6- to 8-week-old female NSG-SGM mice. On day 1, assigned cohorts of tumor-bearing mice were intravenously treated with AAV8-CAG193 (Fig. 1), AAVrh74-EFS193 (Fig. 4), or the AAV-GFP control at $5 \times 10^{12}$ gc/kg by tail vein injection. On day 4, designated cohorts were transplanted with $5 \times 10^6$ huPBMCs from StemExpress (Folsom, CA). For a more aggressive tumor model, $5 \times 10^6$ Raji-Luc/GFP cells were implanted on day 0 in the right flank of 6- to 8-week-old female NSG-SGM mice. On day 3, assigned cohorts of tumor-bearing mice were intravenously treated with AAV8-CAG193 or the AAV-GFP control at $5 \times 10^{12}$ gc/kg by tail vein injection. On day 10, designated cohorts were transplanted with $5 \times 10^6$ huPBMCs. Mice were followed for tumor growth and survival until a humane end point was reached. Tumor growth was determined by measuring tumor bioluminescence (see below) as well as measuring the tumor with calipers and calculating the tumor volume using the formula $l \times w^2 \times \pi/6$. Blood was collected at end point by retro-orbital bleed and analyzed for αCD19-αCD3 dimert concentration as described below.

### Toxicity study

To assess the associated toxicities of continuous systemic expression of the αCD19-αCD3 dimert, $5 \times 10^6$ Raji-Luc/GFP cells were implanted on day 0 in the right flank of 6- to 8-week-old female NSG-SGM mice. On day 1, assigned cohorts of tumor-bearing mice were intravenously treated with AAV with CD19 TransJoin or the GFP control at $5 \times 10^{12}$ gc/kg by tail vein injection. On day 4, designated cohorts were transplanted with $5 \times 10^6$ huPBMCs from StemExpress (Folsom, CA). On day 21, the mice were sedated under 4% isoflurane (Baxter Healthcare, Deerfield, IL) and oxygen (1.5 liters/min; Lindy Gas North America, Bridgewater, NJ) and subjected to exsanguination with euthanasia being confirmed by cervical dislocation. Blood was collected in both Microtainer EDTA (for flow cytometric analysis) and serum-separating tubes (Becton Dickinson, San Jose, CA, USA), allowing the latter to clot at room temperature for 30 min. The clotted blood was centrifuged at 1200*g* for 10 min at room temperature. After collecting the supernatants (serum) and storing at −80°C, the frozen serum samples were shipped to IDEXX BioAnalytics (North Grafton, MA) for analysis on a Mouse Cytokine 25-Panel (62579) and a Standard Toxicology Panel (62794). Heart, kidney, liver, lung, and spleen tissues were harvested for histopathology examination. Briefly, harvested tissues were fixed for 24 hours in 10% buffered formalin (Thermo Fisher Scientific, Waltham, MA), placed in tissue cassettes, and then transferred to 70% ethanol for 24 hours. Fixed tissues were paraffin-embedded by the Morphology

Core at Nationwide Children's Hospital (Columbus, OH). Cutting of serial sections of tissues, hematoxylin and eosin staining, and histopathological evaluations by a licensed veterinary pathologist were performed by IDEXX BioAnalytics (North Grafton, MA).

### Flow cytometric analyses of mouse PBMCs

Peripheral blood (100 μl) from the retro-orbital sinus was collected into EDTA blood collection tubes (BD Biosciences San Jose, CA). Blood samples were mixed with 250 μl of 2% dextran (Sigma-Aldrich, St. Louis, MO) and incubated at 37°C for 30 min to sediment red blood cells. Mononuclear cells in the supernatant were transferred and centrifuged at 400*g*. Contaminating red blood cells were removed by the addition of Ammonium-Chloride-Potassium (ACK) red blood cell lysis buffer (Lonza, Alpharetta, GA). Samples were then blocked with 5% mouse Fc blocking reagent (2.4G2; BD Biosciences) and 5% human Fc blocking reagent (Miltenyi Biotec, Auburn, GA) in fluorescence-activated cell sorting (FACS) buffer [1% FBS and 1 mM EDTA in phosphate-buffered saline (PBS)] before antibody staining. Blocked cells were stained with antibodies against hCD8-allophycocyanin (APC; SK1), mLy-6C-phycoerythrin (PE; AL-21), mLy-6G-Fluorescein isothiocyanate (FITC; 1A8), mF4/80-PE-Cy7 (BM8), hCD4-APC/Cyanine7 (APC-Cy7; SK3), and hCD20–Violet 421 (2H7) at 4°C for 30 min. Labeled cells were washed and fixed in 1% paraformaldehyde (PFA).

### αCD19-αCD3 dimert pharmacokinetics

αCD19-αCD3 dimert serum concentration was determined at end point in efficacy studies and at assigned times in dosing studies. To obtain serum, mice were anesthetized and then subjected to retro-orbital bleeding. End point mice were exsanguinated. Less than 250 μl of blood was obtained every 2 to 3 weeks from the dose study mice. Blood was collected in Microtainer blood collection serum separator tubes with clot activator gel (Becton, Dickinson Co, Franklin Lakes, NJ) and allowed to clot for 30 min. Collection tubes containing blood were centrifuged at 1100*g* for 15 min at room temperature. Next, the serum (supernatant) was collected and stored at <−20°C.

To quantify the concentration of the αCD19-αCD3 dimert in mouse peripheral blood following administration of AAV vectors, serum was thawed and analyzed using the T Cell Activation Bioassay (Promega, Madison, WI) in accordance with the manufacturer's listed protocol. Briefly, mouse sera were diluted 1:4 in RPMI 1640 medium, and 25 μl of these samples was plated in white opaque 96-well plates. Serial dilutions of known concentrations of blinatumomab purchased from Amgen (Thousand Oaks, CA) as 35-mcg injection vials from the Nationwide Children's Hospital Research Pharmacy were also prepared and plated to serve as a standard curve. Diluted serum or a media negative control was added to the coculture of Raji cells and Jurkat TCR/CD3 effector cells in a 96-well plate. After 6 hours of coculture at 37°C, 50 μl of Bio-Glo Luciferase Assay reagent was added to each well and total luminescence was recorded on a Synergy 2 plate reader (BioTek, Winooski, VT) using an integration time of 1 s. Data were analyzed using Prism 8 software to construct a four-parameter logistic curve and interpolate the unknown serum αCD19-αCD3 dimert concentrations against the blinatumomab standards.

Quality control of the sera was performed in conjunction with these assays to retroactively exclude any samples that displayed excessive interference from hemolysis contamination. Following their initial dilution, 25 μl of spare sample was added to 50 μl of RPMI 1640 medium in a clear 96-well plate. Absorbance measurements at 550 nm were then recorded. Any sample with an absorbance of ≥0.02 (a value independently confirmed to maintain ~90% of the resulting luminescent signal of a known standard in the T cell activation assay) was excluded from further analysis.

### In vivo bioluminescent imaging

Bioluminescent imaging was initiated 7 days after implantation of Raji-Luc/GFP tumor cells and conducted weekly thereafter. Each mouse received an intraperitoneal injection of 100 μl (3 mg) of Xenolight Rediject D-luciferin (PerkinElmer, Waltham, MA) and maintained under isoflurane gas anesthesia for 5 min before imaging. Bioluminescent images were obtained using the Xenogen IVIS Spectrum (Caliper Life Sciences, Hopkinton, MA). Quantification of tumor bioluminescent activity was performed with Living Image 4.4 software (PerkinElmer, Waltham, MA) by taking an auto-exposure and recording the total photons in a set region of interest that was kept consistent throughout the duration of study. Bioluminescent activity is presented as photons per second per $cm^2$ per steradian ($p/s/cm^2/sr$). Additional sets of images were taken at 60-s exposures for display purposes in their respective figures.

### Genomic DNA isolation and vector copy number analysis

Harvested tissues were snap-frozen in liquid nitrogen, ground to powder with mortar and pestle, and then stored at −80°C. After processing 25 mg of each tissue (10 mg of spleen) according to the manufacturer's protocol (DNeasy Blood and Tissue Kit, Qiagen, Germantown, MD), genomic DNA was isolated, quantified using a NanoDrop ND-2000 spectrophotometer (Thermo Fisher Scientific, Waltham, MA), and stored at −20°C.

Vector copies per nanogram of tissue were quantified by TaqMan analysis, starting from 100 ng of mouse genomic DNA by amplifying the CD19 TransJoin transgene. The absolute amount of vector was obtained by referring to a standard curve consisting of a 10-fold serial dilution of plasmid pAAV8-CAG193 (six concentrations, ranging from $10^2$ to $10^7$ copies). The absolute number of vector copies is given per 100 ng. The real-time PCR reactions were run with a StepOnePlus Real-Time PCR System using software v2.3 (Applied Biosystems, Foster City, CA). Serial dilutions of the plasmid DNA and 100 ng of purified "sham" high–molecular weight mouse genomic DNA (MilliporeSigma, Burlington, MA) or 100 ng of mouse sample genomic DNA were included in a mix containing TaqMan Universal PCR Master Mix (Applied Biosystems) diluted to 1×, 0.4 μM specific primers, 0.4 μM of the corresponding TaqMan probe, and water to a final volume of 25 μl. The run conditions were as follows: 10 min of 95°C polymerase activation step, followed by 40 cycles of a two-step qPCR (15 s of 95°C denaturation, 1 min of 60°C combined annealing/extension). Primers and probes (5′-3′) were used as follows: *CD3CD19* (forward CTACTGGATGAACTGGGTGAAG; reverse: CTTGAACTTGCCGTTGTAGTTG) and *CD3CD19* probe (/56-FAM/TGGAGTGGA/ZEN/TCGGCCAGATCTG/3IABkFQ/).

### In vitro TransSkip and OncoSkip analyses by RT-PCR

For TransSkip-related studies, 293T cells were seeded in 6- or 12-well plates overnight and then transfected with 1.25 or 2.5 μg of indicated pAAV-193 plasmid using Lipofectamine 3000 (Invitrogen). Twenty-four hours after transfection, antisense morphlino KTS or its sequence-inverted morpholino (GeneTools LLC, Philomath, OR) were delivered to the cultures via Endoporter delivery agent

(GeneTools LLC). For OncoSkip, 3 to $5 \times 10^5$ of the indicated cancer cells were seeded overnight and then KTS or KTSinvert were added to cells via Endoporter. The 293T or cancer cells were harvested 48 hours after morpholino treatment, and their RNA was isolated using the RNeasy Plus Mini Kit (QIAGEN, Germantown, MD). RT was conducted according to the SuperScript IV First-Strand Synthesis System (Invitrogen) for Rh30 and H441 cells and iScript Reverse Transcription Supermix (Bio-Rad) for HeLa. The PCR reactions were then run on a T100 Thermal Cycler (Bio-Rad, Hercules, CA). The conditions were as follows: an initial step at 94°C for 2 min, then up to 40 cycles at 94°C for 30 s, 55°C (54°C for HeLa) for 30 s, and 72°C for 30 s (15 for HeLa), and then a final extension at 72°C for 5 min. Morpholino and primer sequences are listed in Tables 2 and 3, respectively.

### In vitro T and B cell competition binding assays

A total of $5 \times 10^5$ 293T cells were transfected with 1.25 μg of specified AAV-193 plasmid using Lipofectamine 3000 (Invitrogen, Carlsbad CA). After 24 to 48 hours of transfection, culture supernatants were collected for T or B cell binding assays. A total of $3 \times 10^5$ cells of the Jurkat human T leukemia line or the Raji B lymphoma line were preincubated with 5 to 20% of 293T supernatants overnight. After washing with PBS, the cells were blocked with 1% human Fc blocking reagent, stained with hCD19-APC (SJ25C1), or CD3E-PerCp (OKT3) antibody, and chilled on ice for 30 min. Labeled cells were then washed and fixed in 1% PFA. Data for both the PBMC analysis and the T and B cell competition binding assays were collected on a BD FACS LSR II (BD Biosciences) and analyzed using FlowJo software version 10.7.1 (Tree Star, Ashland, OR, USA). All of the staining antibodies were purchased from BioLegend (San Diego, CA, USA) except for anti-human CD19 (eBioscience, San Diego, CA) and anti-mouse Ly-6C (BD Biosciences).

### In vivo TransSkip analysis

At 5 to 6 weeks of age, NSG mice (Envigo, Indianapolis, IN) were intravenously administered AAV8-EFS193 or AAV8-EFS-KM2-193 ($5 \times 10^{12}$ gc/kg) via tail vein injection. Subsequently, these NSG mice were treated with octa-guanidine dendrimer-formed morpholino Vivo-KTS (12.5 mg/kg), its sequence inverted control Vivo-KTSinvert (Vivo-Morpholino, GeneTools, Philomath, OR), or saline was delivered intravenously via tail vein injection for up to two doses, given on two consecutive days for each treatment course. Following peripheral blood harvest by retro-orbital bleed at designated time points, serum was isolated and αCD19-αCD3 pharmacokinetics were assessed as described above. Morpholino sequences are described in Table 2.

### In vivo TransSkip efficacy

The TransSkip antitumor efficacy study was not blinded because of experimental design complexities. Five days before tumor implantation, 6-month-old female NSG-SGM mice were intravenously treated with AAV8-EFS-KM2-193 ($N = 20$) or AAV8-EFS193 ($N = 5$) ($5 \times 10^{12}$ gc/kg). Five days later, $4 \times 10^6$ Raji-Luc/GFP cells were implanted at the right flank. One day after tumor implantation, all the mice were given intravenous injection of $5 \times 10^6$ huPBMCs. In addition, mice treated with AAV8-EFS-KM2-193 were intravenously treated with Vivo-KTS ($n = 10$) or Vivo-KTSinvert (12.5 mg/kg) on days 1 and 2 after tumor implantation. The mice were given repeated treatments of huPBMCs and morpholinos weekly for a total of five cycles. Mice were followed for tumor growth and survival until a humane end point was reached. Tumor growth was determined by measuring the tumor with calipers and calculating the tumor volume as above. Blood was collected every 2 weeks and at end point by retro-orbital bleed and analyzed for αCD19-αCD3 dimert concentration.

**Table 2. Morpholino sequences.**

| Morpholino | Sequence | Figure | Assay |
|---|---|---|---|
| KTS | TAAAACAAGATTTACCTCTATTGTTGGATC | 5, C , and 6, A to B | In vitro TransSkip/OncoSkip |
| KTSinvert | CTAGGTTGTTATCTCCATTTAGAACAAAAT | 5, C and 6, A to B | In vitro TransSkip/OncoSkip |
| Vivo-KTS | TAAAACAAGATTTACCTCTATTGTTGGA | 5, D to G and 6, C to G | In vivo TransSkip |
| Vivo-KTSinvert | AGGTTGTTATCTCCATTTAGAACAAAAT | 5, D to G and 6, C to G | In vivo TransSkip |

**Table 3. Primer sequences for RT-PCR.**

| Name | Sequence | Assay |
|---|---|---|
| TS-Forward | CACCGACTTCACCCTGAACA | TransSkip |
| TS-Reverse | TTGATCTCCAGCTTGGTGCC | TransSkip |
| KRAS Exon0/1-Forward | CATTTCGGACTGGGAGCGAG, | OncoSkip |
| KRAS Exon0/1-Reverse | CTGGTCCCTCATTGCACTGT | OncoSkip |
| KRAS Exon2/3-Forward | TACATGAGGACTGGGGAGGG | OncoSkip |
| KRAS Exon2/3-Reverse | CTTGCTAAGTCCTGAGCCTGT | OncoSkip |
| GAPDH-Forward | AAGGGCATCCTGGGCTACAC | OncoSkip |
| GAPDH-Reverse | TCTTACTCCTTGGAGGCCATGT | OncoSkip |

### Western blot analysis

For OncoSkip, 3 to 5 × $10^5$ of the indicated cancer cells were seeded overnight and then KTS or inverted control morpolinos were added to cancer cells via Endoporter. With primary hepatocytes, 0.9 to 1 × $10^6$ of cells were seeded on collagen-coated six-well plate overnight and then were treated with Vivo-KTS or VivoKTSinvert. Forty-eight hours after morpholino treatment, cells were harvested and whole-cell lysates prepared in cell lysis buffer (9803, Cell Signaling Technology, Danvers, MA) supplemented with protease inhibitor cocktail (Thermo Fisher Scientific, Waltham, MA, USA) and halt phosphatase inhibitor cocktail (P-78420; Thermo Fisher Scientific). After protein concentrations were determined via the Micro BCA Protein Assay Kit (23235; Thermo Fisher Scientific), protein lysates (up to 30 mg) were separated on a denaturing NuPAGE 4 to 12% bis-tris precast gels (NP0336BOX; Thermo Fisher Scientific). The separated proteins were then transferred to polyvinylidene fluoride membrane, blocked for 30 min with blocker casein buffers (PI37582, Thermo Fisher Scientific), and probed overnight at 4°C with the 1:500 dilution of KRAS antibody (clone 4F3, M02A; Abnova, Taipei City, Taiwan) or 1:2000 dilution of anti–glyceraldehyde-3-phosphate dehydrogenase antibody (2118S, Cell Signaling Technology, Danvers, MA, USA). The membranes were washed three times in Tris-buffered saline with 0.1% Tween (TBST) and then probed with a 1:2000 dilution secondary antibody conjugated to horseradish peroxidase (7074S, Cell Signaling Technology). After a series of washes in TBST, the membranes were developed using Western Lightning Plus-ECL reagent (NEL103001EA; PerkinElmer, Waltham, MA) and exposed on x-ray film.

### NEBNext single cell/low input cDNA synthesis

Briefly, 300 ng of total RNA was reverse-transcribed using the NEBNext Single Cell/Low Input Kit for cDNA synthesis following the steps outlined within Iso-Seq Express Template Procedure & Checklist [PN 101-763-800 version 02 (October 2019)]. The resulting cDNA was purified and size-selected at >1.0 kb using 1.0× ProNex beads (Promega, Madison, WI) with a final elution of 17 μl in buffer EB (elution buffer) (QIAGEN, Hilden, Germany). Subsequent PCR amplification used Takara PrimeStar GXL DNA polymerase (2.50 U total) with NEBNext Single Cell (catalog no. E6421S) and Iso-Seq Express (PN no. 101-737-500) cDNA primers; primer binding site incorporation occurred during first-strand cDNA synthesis. Sample cDNA amplification occurred in duplicate in 50 μl of PCR reactions with each containing 8 μl of purified first-strand cDNA template, 1× PrimeSTAR GXL buffer, 0.1 mM deoxynucleotide triphosphates, 1.25 U of PrimeSTAR GXL DNA polymerase (1.25 U/μl), and 1 μl of NEBNext Single Cell and Iso-Seq Express cDNA PCR primers. PCR cycling conditions were as follows: 30 s at 98°C, 15 cycles (10 s at 98°C, 15 s at 65°C, and 10 min at 68°C), and 5 min at 68°C.

### cDNA size fractionation

Combining duplicate PCR reactions after amplification allowed for >2-kb size selection using 0.4× and 0.4/0.6× ratios of SPRIselect paramagnetic beads (Beckman Coulter, Brea, CA). Supernatant from the 0.4× sizing was added to 20 μl of SPRI select beads yielding a double-sided size-selected product between 0.5 and 2 kb. Bead-associated cDNA was eluted and concentrated in 12 μl of buffer EB. Pooling the fractionated size-selected cDNA (final yield of 500 ng) at a 1:1 molar ratio of >2 kb (0.4×) and 0.5 to 2 kb (0.4/0.6×) fractions allowed for equal representation of the larger-sized molecules during PacBio SMRT cell loading and sequencing.

### SMRTbell template prep and Sequel II sequencing

SMRTbell library preparation of the pooled cDNA fractions used the SMRTbell Express Template Prep Kit 2.0 according to PacBio Iso-Seq protocol [PN 101-763-800 version 02 (October 2019)]. A fivefold dilution derived from the final SMRTbell library was used for assessing concentration and average library size by Qubit dsDNA HS and the 2100 Bioanalyzer High Sensitivity DNA Kit (Agilent), respectively. Volumetric calculations were done on a per-sample basis using SMRT Link Sample Setup for v4 primer and polymerase binding conditions dependent on initial SMRTbell library molarity. SMRTbell libraries were complexed with the Sequel II Binding Kit 2.0, purified with 1.0× ProNex beads, and sequenced at 60 pM on-plate loading concentration. Samples were sequenced on a single 8 M SMRT cell on the PacBio Sequel IIe platform using v2.0 chemistries. Sequencing included a 2-hour pre-extension and a 24-hour movie collection. The PacBio long-read RNA sequencing (Iso-Seq) data presented in this publication have been deposited in National Center for Biotechnology Information's (NCBI's) Sequence Read Archive and is available through accession number PRJNA752121.

### Statistical analyses

Statistical analyses for continuous measures were performed using the GraphPad Prism software 7.0a for Mac OS X (GraphPad Software, La Jolla, CA, USA), and survival data were analyzed using SAS (SAS Institute, Cary, NC). Kaplan-Meier curves and corresponding log-rank Mantel-Cox tests were used to evaluate the statistical differences between groups in survival studies. One-way analysis of variance was used to assess the statistical difference between groups in the flow cytometry analyses. Multiplicity was adjusted by Bonferroni method to control type I error. For Fig. 4G, smoothed splines were fit to visualize the general nonlinear trend of blinatumomab equivalents over time. For Fig. 5F, tumor growth data were analyzed by using mixed-effects modeling, accounting for observational dependencies for each tumor. SAS 9.4 software (SAS Institute, Cary, NC) was used for analysis. For Fig. 5G, data were analyzed using survival with competing event (death not due to tumor) analysis. Because of the high rate of early graft-versus-host disease in this experiment, death not associated with tumor was considered to be competing risk. The comparisons of cumulative incidence rates among groups were conducted by Gray's test (*34*). SAS 9.4 software (SAS Institute, Cary, NC) was used for analysis.

## REFERENCES AND NOTES


1. F. Le Gall, U. Reusch, M. Little, S. M. Kipriyanov, Effect of linker sequences between the antibody variable domains on the formation, stability and biological activity of a bispecific tandem diabody. *Protein Eng. Des. Sel.* **17**, 357–366 (2004).
2. M. Zhu, B. Wu, C. Brandl, J. Johnson, A. Wolf, A. Chow, S. Doshi, Blinatumomab, a bispecific T-cell engager (BiTE®) for CD-19 targeted cancer immunotherapy: Clinical pharmacology and its implications. *Clin. Pharmacokinet.* **55**, 1271–1288 (2016).
3. G. Guler-Gane, S. Kidd, S. Sridharan, T. J. Vaughan, T. C. Wilkinson, N. J. Tigue, Overcoming the refractory expression of secreted recombinant proteins in mammalian cells through modification of the signal peptide and adjacent amino acids. *PLOS ONE* **11**, e0155340 (2016).
4. M. Wunderlich, F. S. Chou, C. Sexton, P. Presicce, C. A. Chougnet, J. Aliberti, J. C. Mulloy, Improved multilineage human hematopoietic reconstitution and function in NSGS mice. *PLOS ONE* **13**, e0209034 (2018).
5. Y. Hijazi, M. Klinger, A. Kratzer, B. Wu, P. A. Baeuerle, P. Kufer, A. Wolf, D. Nagorsen, M. Zhu, Pharmacokinetic and pharmacodynamic relationship of blinatumomab in patients with non-hodgkin lymphoma. *Curr. Clin. Pharmacol.* **13**, 55–64 (2018).
6. G. Ehx, J. Somja, H. J. Warnatz, C. Ritacco, M. Hannon, L. Delens, G. Fransolet, P. Delvenne, J. Muller, Y. Beguin, H. Lehrach, L. Belle, S. Humblet-Baron, F. Baron, Xenogeneic graft-versus-host disease in humanized NSG and NSG-HLA-A2/HHD mice. *Front. Immunol.* **9**, 1943 (2018).

7. U. P. Dave, K. Cornetta, AAV joins the rank of genotoxic vectors. *Mol. Ther.* **29**, 418–419 (2021).
8. S. K. Powell, R. Rivera-Soto, S. J. Gray, Viral expression cassette elements to enhance transgene target specificity and expression in gene therapy. *Discov. Med.* **19**, 49–57 (2015).
9. A. Fernandez-Medarde, E. Santos, Ras in cancer and developmental diseases. *Genes Cancer* **2**, 344–358 (2011).
10. J. R. Mendell, S. A. Al-Zaidy, L. R. Rodino-Klapac, K. Goodspeed, S. J. Gray, C. N. Kay, S. L. Boye, S. E. Boye, L. A. George, S. Salabarria, M. Corti, B. J. Byrne, J. P. Tremblay, Current clinical applications of in vivo gene therapy with AAVs. *Mol. Ther.* **29**, 464–488 (2021).
11. C. G. Chisari, E. Sgarlata, S. Arena, S. Toscano, M. Luca, F. Patti, Rituximab for the treatment of multiple sclerosis: A review. *J. Neurol.* **269**, 159–183 (2022).
12. C. Breton, T. Furmanak, A. N. Avitto, M. K. Smith, C. Latshaw, H. Yan, J. A. Greig, J. M. Wilson, Increasing the specificity of AAV-based gene editing through self-targeting and short-promoter strategies. *Mol. Ther.* **29**, 1047–1056 (2021).
13. W. L. Chew, Immunity to CRISPR Cas9 and Cas12a therapeutics. *Wiley Interdiscip. Rev. Syst. Biol. Med.* **10**, e1408 (2018).
14. H. Adachi, M. Hengesbach, Y. T. Yu, P. Morais, From antisense RNA to RNA modification: Therapeutic potential of RNA-based technologies. *Biomedicine* **9**, 550 (2021).
15. H. Kantarjian, A. Stein, N. Gokbuget, A. K. Fielding, A. C. Schuh, J. M. Ribera, A. Wei, H. Dombret, R. Foa, R. Bassan, O. Arslan, M. A. Sanz, J. Bergeron, F. Demirkan, E. Lech-Maranda, A. Rambaldi, X. Thomas, H. A. Horst, M. Bruggemann, W. Klapper, B. L. Wood, A. Fleishman, D. Nagorsen, C. Holland, Z. Zimmerman, M. S. Topp, Blinatumomab versus chemotherapy for advanced acute lymphoblastic leukemia. *N. Engl. J. Med.* **376**, 836–847 (2017).
16. N. Gokbuget, H. Dombret, M. Bonifacio, A. Reichle, C. Graux, C. Faul, H. Diedrich, M. S. Topp, M. Bruggemann, H. A. Horst, V. Havelange, J. Stieglmaier, H. Wessels, V. Haddad, J. E. Benjamin, G. Zugmaier, D. Nagorsen, R. C. Bargou, Blinatumomab for minimal residual disease in adults with B-cell precursor acute lymphoblastic leukemia. *Blood* **131**, 1522–1531 (2018).
17. A. Viardot, M. E. Goebeler, G. Hess, S. Neumann, M. Pfreundschuh, N. Adrian, F. Zettl, M. Libicher, C. Sayehli, J. Stieglmaier, A. Zhang, D. Nagorsen, R. C. Bargou, Phase 2 study of the bispecific T-cell engager (BiTE) antibody blinatumomab in relapsed/refractory diffuse large B-cell lymphoma. *Blood* **127**, 1410–1416 (2016).
18. M. Zhu, A. Kratzer, J. Johnson, C. Holland, C. Brandl, I. Singh, A. Wolf, S. Doshi, Blinatumomab pharmacodynamics and exposure-response relationships in relapsed/refractory acute lymphoblastic leukemia. *J. Clin. Pharmacol.* **58**, 168–179 (2018).
19. K. C. Pehlivan, B. B. Duncan, D. W. Lee, CAR-T cell therapy for acute lymphoblastic leukemia: Transforming the treatment of relapsed and refractory disease. *Curr. Hematol. Malig. Rep.* **13**, 396–406 (2018).
20. X. Li, W. Chen, Mechanisms of failure of chimeric antigen receptor T-cell therapy. *Curr. Opin. Hematol.* **26**, 427–433 (2019).
21. S. Depil, P. Duchateau, S. A. Grupp, G. Mufti, L. Poirot, 'Off-the-shelf' allogeneic CAR T cells: Development and challenges. *Nat. Rev. Drug Discov.* **19**, 185–199 (2020).
22. A. Perales-Puchalt, E. K. Duperret, X. Yang, P. Hernandez, K. Wojtak, X. Zhu, S. H. Jung, E. Tello-Ruiz, M. C. Wise, L. J. Montaner, K. Muthumani, D. B. Weiner, DNA-encoded bispecific T cell engagers and antibodies present long-term antitumor activity. *JCI Insight* **4**, e126086 (2019).
23. J. P. W. Heidbuechel, C. E. Engeland, Oncolytic viruses encoding bispecific T cell engagers: A blueprint for emerging immunovirotherapies. *J. Hematol. Oncol.* **14**, 63 (2021).
24. H. Khalique, R. Baugh, A. Dyer, E. M. Scott, S. Frost, S. Larkin, J. Lei-Rossmann, L. W. Seymour, Oncolytic herpesvirus expressing PD-L1 BiTE for cancer therapy: Exploiting tumor immune suppression as an opportunity for targeted immunotherapy. *J. Immunother. Cancer* **9**, e001292 (2021).
25. B. D. Choi, X. Yu, A. P. Castano, A. A. Bouffard, A. Schmidts, R. C. Larson, S. R. Bailey, A. C. Boroughs, M. J. Frigault, M. B. Leick, I. Scarfo, C. L. Cetrulo, S. Demehri, B. V. Nahed, D. P. Cahill, H. Wakimoto, W. T. Curry, B. S. Carter, M. V. Maus, CAR-T cells secreting BiTEs circumvent antigen escape without detectable toxicity. *Nat. Biotechnol.* **37**, 1049–1058 (2019).
26. M. W. Bolt, J. T. Brady, L. O. Whiteley, K. N. Khan, Development challenges associated with rAAV-based gene therapies. *J. Toxicol. Sci.* **46**, 57–68 (2021).
27. A. S. Stein, R. A. Larson, A. C. Schuh, W. Stevenson, E. Lech-Maranda, Q. Tran, Z. Zimmerman, W. Kormany, M. S. Topp, Exposure-adjusted adverse events comparing blinatumomab with chemotherapy in advanced acute lymphoblastic leukemia. *Blood Adv.* **2**, 1522–1531 (2018).
28. A. Lin, A. B. Balazs, Adeno-associated virus gene delivery of broadly neutralizing antibodies as prevention and therapy against HIV-1. *Retrovirology* **15**, 66 (2018).
29. E. Kampouri, C. S. Walti, J. Gauthier, J. A. Hill, Managing hypogammaglobulinemia in patients treated with CAR-T-cell therapy: Key points for clinicians. *Expert Rev. Hematol.* **15**, 305–320 (2022).
30. N. Iwamoto, D. C. D. Butler, N. Svrzikapa, S. Mohapatra, I. Zlatev, D. W. Y. Sah, Meena, S. M. Standley, G. Lu, L. H. Apponi, M. Frank-Kamenetsky, J. J. Zhang, C. Vargeese, G. L. Verdine, Control of phosphorothioate stereochemistry substantially increases the efficacy of antisense oligonucleotides. *Nat. Biotechnol.* **35**, 845–851 (2017).
31. U. Burki, J. Keane, A. Blain, L. O'Donovan, M. J. Gait, S. H. Laval, V. Straub, Development and application of an ultrasensitive hybridization-based ELISA method for the determination of peptide-conjugated phosphorodiamidate morpholino oligonucleotides. *Nucleic Acid. Ther.* **25**, 275–284 (2015).
32. K. Stieger, B. Belbellaa, C. Le Guiner, P. Moullier, F. Rolling, In vivo gene regulation using tetracycline-regulatable systems. *Adv. Drug Deliv. Rev.* **61**, 527–541 (2009).
33. G. Zhong, H. Wang, W. He, Y. Li, H. Mou, Z. J. Tickner, M. H. Tran, T. Ou, Y. Yin, H. Diao, M. Farzan, A reversible RNA on-switch that controls gene expression of AAV-delivered therapeutics in vivo. *Nat. Biotechnol.* **38**, 169–175 (2020).
34. R. J. Gray, A class of K-sample tests for comparing the cumulative incidence of a competing risk. *Ann. Stat.* **16**, 1141–1154 (1988).


**Acknowledgments:** We thank pathologist K. N. Corps, DVM, PhD (The Ohio State University) for analyses of mouse tissues; E. Frair and N. Rohan for technical assistance; A. Studebaker, A. Kohler, and A. Ivanovic for the help with blinding; S. McGrath for PacBio processing; and A. Gupta (Roswell Park) for critical review. Drawings were created in Biorender.com. **Funding:** This work was supported by the Department of Defense award W81XWH-19-1-0371 (to T.P.C.), Nationwide Children's Hospital Technology Development Fund, the Ohio Development Services Agency and Third Frontier Technology Validation and Start-Up Fund, and the Cancer Free Kids Pediatric Cancer Research Alliance. This work was also supported by an RNA Fellowship from the Center for RNA Biology at The Ohio State University (to A.S.V.), the Ohio State University Comprehensive Cancer Center and the National Institutes of Health (P30 CA016058), National Cancer Institute Cancer Moonshot Award U54-CA232561-01A1 (to T.P.C. and E.R.M.), National Cancer Institute R01 CA262873 (to D.S.C.), and National Cancer Institute R03 CA259865 (to D.S.C.).
**Author contributions:** Conceptualization: T.P.C., J.R.M., V.M., and E.R.M. Methodology: T.P.C., B.H., M.A.C., C.-Y.C., A.R.M., S.W., V.M., D.S.C., and P.-Y.W. Validation, X.M., and J.R.S. Formal analysis: X.M. and J.R.S. Investigation: B.H., M.A.C., C.-Y.C., A.M.G., G.C.S., J.M.H., M.R.D., A.S.V., and P.-Y.W. Resources: E.R.M. and J.R.M. Data curation: B.H., M.A.C., C.-Y.C., A.R.M., S.W., and P.-Y.W. Writing—original draft: T.P.C. Writing—review and editing: B.H., M.A.C., C.-Y.C., E.R.M., J.R.M., D.S.C., and P.-Y.W. Visualization: B.H. and X.M. Supervision: T.P.C., V.M., E.R.M., J.R.M., and D.S.C. Project administration: T.P.C. Funding acquisition, T.P.C., E.R.M., J.R.M., and D.S.C.
**Competing interests:** The technology described here is the subject of international patent application WO2020172259A1 with T.P.C., B.H., M.A.C., C.-Y.C., D.S.C., and P.-Y.W. as inventors and exclusively licensed to Vironexis Biotherapeutics Inc. with T.P.C., B.H., M.A.C., C.-Y.C., and P.-Y.W. holding common stock. The authors declare that they have no other competing interests.
**Data and materials availability:** The PacBio long-read RNA sequencing (Iso-Seq) data presented in this publication have been deposited in NCBI's Sequence Read Archive (SRA) and are available through accession number PRJNA752121 using the following link: https://urldefense.com/v3/__https://www.ncbi.nlm.nih.gov/Traces/study/?acc=PRJNA752121__;!!NiUAmZJ8c1GNWg!TeX3S_ztXjREE8eirgrneZZOrKJ2AiMMkL8M2DaoNC8_cX-79-Nd3RZ--6ON8v0OFHApfnEplO5HWsL-wtmU5FKwmlvZ8-nt-3VJ1A$. All data needed to evaluate the conclusions in the paper are present in the paper. The plasmids and rAAVs reported here can be provided by Nationwide Children's Hospital pending scientific review and a completed material transfer agreement, provided the request does not conflict with other superseding licensing agreements. Requests for these materials should be submitted to T.P.C. (timothy.cripe@nationwidechildrens.org).

Submitted 31 August 2021
Accepted 27 May 2022
Published 13 July 2022
10.1126/sciadv.abm1890